Cont. Mech. Therm. doi.10.1007/s00161-019-00747-5 manuscript No.
(will be inserted by the editor)

M. Hossain

Modelling the curing process in particle-filled electro-active polymers with a dispersion anisotropy

Received: 01 August 2018 / Accepted: 19 January 2019

Abstract Even for a moderate actuation, a large electric voltage requirement hinders the application of electro-active polymers (EAPs) in many areas. Hence, among other mechanisms, the actuation enhancement in EAPs is performed via inclusions of high dielectric permittivity fillers in the matrix material in the uncured stage. Moreover, to obtain an optimum advantage from the high dielectric permittivity fillers, an electric field can be applied during the curing process which helps the particles to align in a preferred direction. To be specific, recent experimental evidences show that these particles form a dispersed anisotropy rather than a perfect transverse anisotropic structure. The polymer curing process is a complex (visco-) elastic phenomenon where a liquid polymer gradually transforms into a solid macromolecular structure due to cross-linking of the initial solution of short polymer chains. This phase transition comes along with an increase in the material stiffness and a volume shrinkage. In this paper we present a phenomenologically-inspired large strain framework for simulating the curing process of particle-filled electro-active polymers with a dispersion-type anisotropy that can work under the influence of an electro-mechanically coupled load. The application of the proposed approach is demonstrated with some numerical examples. These examples illustrate that the model can predict common features in particle-filled dispersed electro-active polymers undergoing curing processes in the presence of an electro-mechanically coupled load.

Keywords Electro-active polymers · polymer curing · electro-mechanical coupled problem · dispersion anisotropy · electro-elasticity · curing shrinkage

Mokarram Hossain
Zienkiewicz Centre for Computational Engineering, College of Engineering, Swansea University, SA1 8EN, Fabian Way, United Kingdom
Tel.:+44-7482959957
E-mail: mokarram.hossain@swansea.ac.uk

1 Introduction

Among other functional materials, electro-active polymers (EAPs) draw considerable attention due to their many exotic properties, e.g., large and complex actuations, compared to classical infinitesimally-actuated smart materials [37; 55]. EAPs have potential applications in stretch sensors, actuator and energy harvesters. In the case of transducers, an electric load converts into a mechanical energy and vice-versa. In modelling such problems, governing equations need to be solved as coupled problems since EAPs exhibit an electro-mechanical coupling behaviour, cf. [68; 10]. The excitations on EAPs by an externally applied electric field result in large deformations and a change in their internal material behaviour. Depending on the mechanism for the deformation, EAPs can be divided into two major categories: electronic electro-active polymers (EEAPs) and ionic electro-active polymers. In EEAPs, two electro-mechanical forces are mainly responsible for the deformation of the polymer; (i) the so-called Maxwell stress that originates due to electric field and penetrates free space and matter alike and (ii) the electrostriction that is due to intramolecular electrostatic forces of the material, see Vogel [67], Monk [47].

1.1 Modelling electro-elasticity

For modelling the electro-elastic coupled behaviour of electro-active polymers, several research works appeared in the literature. Some of the pioneering works in the finite strain electro-elasticity are due to Dorfmann and Ogden [10; 11] which are further extended by Bustamante [6] in the case of transverse isotropy. Another of the seminal works in the area is due to Wissler et al. [69] where the authors formulated their constitutive models in line with the so-called quasi-linear viscoelasticity. More recently, Ask and co-workers [3] modelled the electrostrictive behaviours of viscoelastic polymers using a phenomenologically-motivated constitutive ansatz. In contrast to earlier works in the area, Ask and co-workers validated their electro-viscoelastic models with experimental data of Johlitz et al. [36] and Diaconu et al. [12]. Exploiting the classical work of finite strain nonlinear viscoelasticity proposed by Reese and Govindjee [56], Büschel and co-workers [5] proposed an electro-viscoelastic model using a multiplicative decomposition of the deformation gradient into an elastic part and a viscous part for the mechanical deformation. In this work, they considered only a time-dependent evolution for the mechanical internal variable and the electric quantity does not evolve with time.

Vogel [67] proposed an electro-viscoelastic model for EAPs where the governing kinematical and constitutive equations were formulated in the logarithmic strain-space. The author formulated the constitutive relation considering the influence of the electric field also on viscous responses. With a few illustrative numerical examples they conclude that the electric field affects not only the equilibrium part of the energy function but also the viscous part, usually known as the non-equilibrium response. Similar to Vogel [67], Saxena et al.

[62] proposed an electro-viscoelastic coupled model that considered the electric field influence also on the non-equilibrium part. In this case, Saxena and co-workers [62] decomposed the electric variable, i.e. electric field, into an elastic part and a viscous part. This decomposition idea is in line with the so-called multiplicative decomposition of the deformation gradient, a well-known concept in viscoelastic and viscoplastic areas. Moreover, a thermodynamically consistent evolution law is proposed for tracking the electric internal variable evolution which is absent in the model proposed by Vogel [67]. All constitutive models discuss above describing the electro-active response of dielectric elastomers are based on the so-called phenomenological approach. Hence, very recently few efforts are made in formulating micro-mechanically motivated electro-elastic models. Itskov et al. [35] proposed an electromechanical constitutive model based on molecular chain statistics that considered polarization of single polymer chain segments and took into account their directional distribution. They argued that the derived constitutive formulations resulted in a small number of physically interpretable material constants.

1.2 Enhancement of electro-active polymers

Despite many promising features of EAPs, a high electric voltage requirement, even for a moderately actuated deformation, restricts their applications in many areas especially in the areas where human interactions are predominant. Moreover, high voltage demands result in a large instrumentation and a higher cost. Hence, the actuation enhancement for EAPs has been an active field of research for the last two decades. To increase actuation, sensing and energy harvesting by increasing dielectric permittivities, several strategies are currently available in the literature [7; 8; 13; 19; 70; 45; 38; 39; 48; 52; 57; 58; 59; 65; 70]. Among other procedures, the inclusion of high dielectric permittivity fillers into the polymeric matrix results in a higher deformation with a reduced amount of voltage. According to Dang et al. [13], for the enhancement of transducers, the particle inclusion option is one of the most investigated procedures in the literature. These dielectric permittivity enhancement methods can be classified into three main groups: random composites, field-structured composites, and new synthesised polymers [8]. In the first approach, a filler, either in a powder form or in a liquid form, is dispersed into a polymeric matrix. The fillers can be of various scales, e.g. nanoscale to micro-scale. Some commonly used fillers are, e.g., titanium dioxide, lead magnesium niobate, lead titanate. Very recently, Carbon Nano Tube (CNT)-filled EAP composites gain a significant attention due to their excellent electric properties over other particle-filled transducer materials [59]. The fillers of high dielectric constant are usually introduced in the form of powder in the elastomeric matrix before the curing process starts. In general, the resulting composites will have intermediate dielectric properties with respect to those of either matrix or filler [19]. In the second method, the fillers are also used to make a composite material. However, the material is now cured in the presence of an externally applied electric field in order to align the fillers in a preferred

direction. Such an alignment of dipoles under the application of an electric field increases electric polarization and hence the polarization stress [38]. Recent experimental evidences [38] suggest that the application of an electric field during the curing process results in better actuations. The third strategy of the dielectric permittivity enhancement is to synthesise new materials with tailored characteristics. In this case, the addition of specific chemical agents alters the internal structures of polymers.

1.3 Scopes of the present work

Several experimental works demonstrate the formation of homogeneously distributed particle-filled isotropic EAP composites where there is no application of an external electric field during the curing process [39; 8; 45; 38; 40]. However, the application of an external electric field during the process yields a field-structured composite where the axis of anisotropy is along the direction of the applied electric field. To be specific, such an alignment of chains is not forming a perfect anisotropy rather it has a dispersion along the mean direction, see for example Fig (3) in Kashani et al. [38] for ceramic-filled EAP composites while anisotropic CNT-filled EAPs are presented in Oliva et al. [53]. A great amount of efforts is devoted to find homogenised properties of EAP composites using multi-scale techniques [40]. In deriving homogenised properties, it is roughly assumed that there is a perfect bonding between the fillers and the matrix materials during the entire curing process. However, the fully-cured final properties of these composite materials largely depend on the duration, nature and effects of the curing process. For example, in the case of particle-filled EAP preparations, the uneven or differential curing (typically known as the warpage) inside a mould of the composites is a common phenomenon that might create residual stresses. This undesirable warpage will be significant if the thickness of a sample becomes considerably large. Secondly, the formation of new chemical bonds during the curing allows the chains to come closer that results in a decrease in specific volume which is denoted as the volume or the curing shrinkage. The shrinkage-generated stresses can eventually de-bond composites from the mould if the bond strength between the mould and the composite is not strong enough. Thirdly, most of the curing reactions are either exothermic or endothermic. Hence, the lack of proper and timely dissipation of the generated heat across the mould is further responsible for a spatial and temporal stress evolution in the matrix. In such cases, cure-dependent electro-mechanically coupled constitutive models implemented in a simulation framework can be useful tools to predict and to minimise such expected but unwanted pathological phenomena.

To the best of the authors' knowledge, there is currently no constitutive model that can capture the stiffness gaining process of polymeric composites with a dispersed anisotropy in the presence of an electro-mechanically coupled load. Hence, a finite strain framework is required to predict the curing process with an electro-mechanically coupled field. In order to capture all relevant phenomena during a purely mechan-

ical curing, several authors have proposed phenomenologically-inspired curing models for small and finite strains, see for example, Kiasat [41], Lion et al. [44], Hossain et al. [21; 22; 23], Landgraf et al. [42; 43], Heinrich et al. [32], Mahnken [50]. For a further review on the constitutive modelling of purely mechanical curing process of polymers, our previous contributions, i.e. Hossain et al. [21; 22; 23] can be considered. Uncured rubber demonstrates viscoplastic behaviours in the absence of distinct yield point. Hence, due to lack of proper crosslinks, classical hyperelastic models do not apply to uncured rubber. Very recently, Dal et al. [14] proposed a constitutive model for the isothermal response of uncured green rubber. Recently, Hossain et al. [26; 27] proposed a finite strain framework for the stiffness gaining for particle-filled magneto-active materials which is further extended in Hossain et al. [25] for EAP composites. However, these constitutive models did not take into account the dispersion anisotropy that is experimentally observed in EAPs composites when they are being cured under an electric field. Therefore, the aim of the current contribution is to formulate an electro-mechanically coupled curing model that can take into account the chain dispersions in EAP composites. The model will be based on the hypoelastic concept (rate-form) of our previously proposed mechanical and coupled curing models [22; 23].

The paper is organized in the following way. Section 2 will briefly review an electro-elastic model for fully-cured elastomers that basically originates from a recently proposed electro-mechanical model by our group. In Section 3, the main mathematical procedure is described that leads to a generic constitutive relation for the polymer curing process in the presence of an electro-mechanically coupled load. In Section 4, a novel approach is proposed to capture the curing-induced volume shrinkage. This procedure is an extension of the multiplicative decomposition of the deformation gradient-based approach to the dispersion-type anisotropic curing shrinkage where the dispersion effect is scaled via a von Mises distribution function. The evolution of the various time-dependent material parameters appearing in the free energy function is discussed in the same section. Section 5 discusses a specific energy function to verify the constitutive framework developed in Section 3. The final Section 6 presents some numerical examples which illustrate that the proposed model can capture relevant phenomena of polymer curing in the presence of an electro-mechanically coupled field.

2 Modelling dispersion anisotropy in electro-active polymers

In particle-filled EAPs that are cured under an electric field, we assume that the orientations of the chains within a family I (with $I = 1 \cdots N$) are distributed by a certain dispersion with respect to a mean preferred direction. A schematic figure of such a dispersion is depicted in Fig 1. Such a family of chains constitutes a transversely isotropic contribution to the overall response of EAP composites. Hence, the chain contributions are added to the bulk part of the free energy. The incorporation of the dispersed chain contributions to the over-

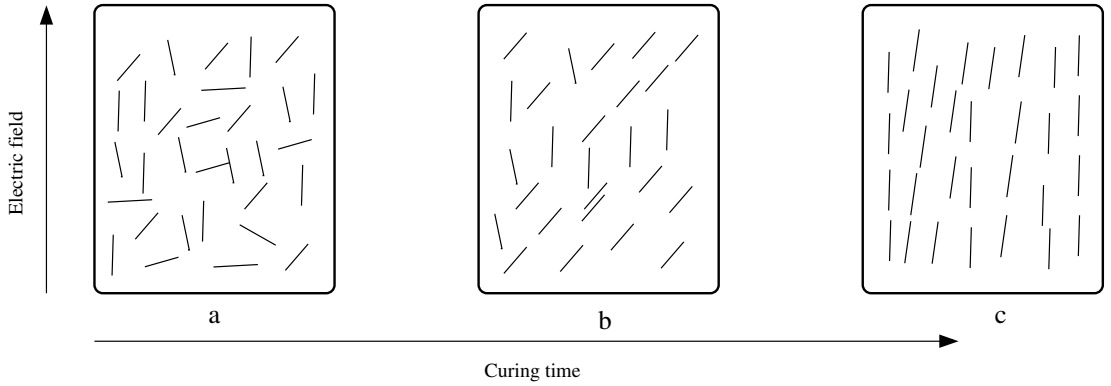

Fig. 1: A schematic representation of the curing process in particle-filled EAPs under an electric field: a) Initial random distribution of the particles embedded in a monomeric solution (not shown here), b) Particles are gradually aligned in the direction of the applied field, c) Particles form dispersed anisotropic structures under the field

all free energy function in the case of electro-mechanically coupled problems in fully-cured electro-elasticity is formulated in our recent contribution, see Hossain and Steinmann [31]. For the sake of completeness, we provide a brief summary of the modelling framework here. Therein, the averaging process of transferring the free energy contribution of single chains from the microscopic level to the macroscopic continuum level is done as

$$\bar{\boldsymbol{t}} = \bar{\boldsymbol{F}}\boldsymbol{r}, \tag{1}$$

where $\bar{\boldsymbol{F}}(= J^{-\frac{1}{3}}\boldsymbol{F}$, $\boldsymbol{F}$ is the deformation gradient and $J = \det\boldsymbol{F})$ is isochoric deformation gradient and $\boldsymbol{r}$ is the orientation vector representing a single chain. Then the macro-stretch $\bar{\lambda}$ of a material line element is defined relating the orientation vector $\bar{\boldsymbol{t}}$ as

$$\bar{\lambda} = |\bar{\boldsymbol{t}}| = \sqrt{\bar{\boldsymbol{t}} \cdot \bar{\boldsymbol{t}}} = \sqrt{\bar{\boldsymbol{F}}\boldsymbol{r} \cdot \bar{\boldsymbol{F}}\boldsymbol{r}} = \sqrt{\bar{\boldsymbol{C}} : [\boldsymbol{r} \otimes \boldsymbol{r}]}, \tag{2}$$

where $\bar{\boldsymbol{C}} = \bar{\boldsymbol{F}}^T\bar{\boldsymbol{F}}$ is the isochoric right Cauchy-Green deformation tensor, see Miehe et al. [49]. Similarly, the electric field vector is projected onto the direction of the chain $\boldsymbol{r}$ to obtain a chain-oriented scalar electric field E as

$$E = \mathbb{E} \cdot \boldsymbol{r}, \tag{3}$$

where $\mathbb{E}$ is the electric field vector in the material configuration, see Thylander [66]. Following the classical approach of decoupled representation of the strain energy in polymeric materials into a volumetric and an isochoric part, a similar analogy is adopted in the electro-elasticity as

$$\Psi = \Psi_{\text{vol}}(J) + \Psi_{\text{iso}}(\bar{\boldsymbol{C}}, \mathbb{E}, \boldsymbol{a}_1, \cdots, \boldsymbol{a}_N) = \Psi_{\text{vol}}(J) + \Psi^{\text{isp}}_{\text{iso}}(\bar{\boldsymbol{C}}, \mathbb{E}) + \Psi^{\text{ani}}_{\text{iso}}(\bar{\boldsymbol{C}}, \mathbb{E}, \boldsymbol{a}_1, \cdots, \boldsymbol{a}_N) \tag{4}$$

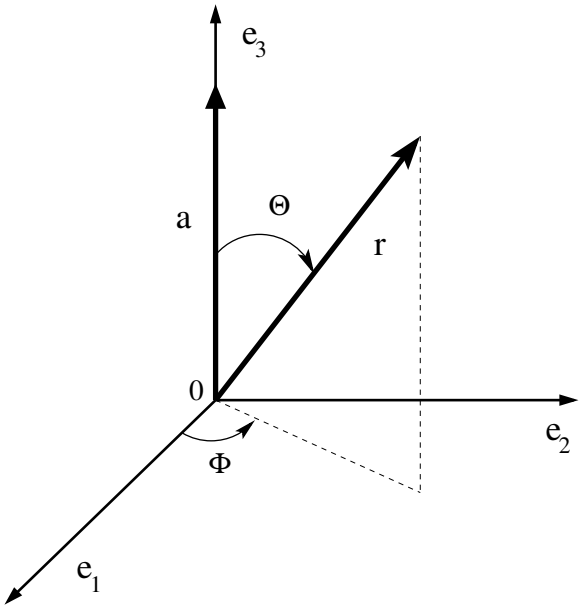

Fig. 2: The representation of a single chain $\boldsymbol{r}$ in the three-dimensional space. Additionally, the preferential unit vector $\boldsymbol{a}$ is oriented in a way so that it coincides with the Cartesian coordinate axis $\boldsymbol{e}_3$

where $\Psi_{\text{vol}}(J)$ is the volumetric and Ψ_{iso} is the isochoric energy functions, respectively. Here the array of vectors, i.e., $\boldsymbol{a}_1, \cdots, \boldsymbol{a}_N$ represent the N families of chains. The isochoric energy Ψ_{iso} is further decomposed into an isotropic part $\Psi_{\text{iso}}^{\text{isp}}$ and an anisotropic part $\Psi_{\text{iso}}^{\text{ani}}$, respectively. Each chain orientation is expressed by an arbitrary unit vector $\boldsymbol{r}(\Theta, \Phi) = \sin\Theta\cos\Phi\boldsymbol{e}_1 + \sin\Theta\sin\Phi\boldsymbol{e}_2 + \cos\Theta\boldsymbol{e}_3$ ($\boldsymbol{r} \in \mathbb{U}^2$, $|\boldsymbol{r}| = 1$) . Therein, the unit vector is characterized by the use of Eulerian angles $\Theta \in [0, \pi]$, $\Phi \in [0, 2\pi]$ and $\{\boldsymbol{e}_i\}_{i=1,2,3}$ denote the axes of a rectangular Cartesian coordinate system, cf. Fig (2). Similar to the chain orientation vector $\boldsymbol{r}$, the preferential vector $\boldsymbol{a}$ can also be expressed in terms of the Eulerian angles, i.e., $\boldsymbol{a}(\Theta^{\text{m}}, \Phi^{\text{m}}) = \sin\Theta^{\text{m}}\cos\Phi^{\text{m}}\boldsymbol{e}_1 + \sin\Theta^{\text{m}}\sin\Phi^{\text{m}}\boldsymbol{e}_2 + \cos\Theta^{\text{m}}\boldsymbol{e}_3$, where $\Theta^{\text{m}} \in [0, \pi]$ and $\Phi^{\text{m}} \in [0, 2\pi]$, cf. Fig 2.

Now the macroscopic energy density is derived from the microscopic contributions of single chain energy densities. We consider N preferred (mean) orientations $\boldsymbol{a}_1, \cdots, \boldsymbol{a}_N$ related to N families of chains and each family of chains is symmetrically distributed along a preferred direction $\boldsymbol{a}_I \in \mathbb{U}^2$. Furthermore, if it is assumed that n number of chains exist per unit volume, then the anisotropic part of the macroscopic electromechanical coupled energy for this set of chains is obtained as

$$\Psi_{\text{iso}}^{\text{ani}}(\bar{\boldsymbol{C}}, \mathbb{E}, \boldsymbol{a}_1, \cdots, \boldsymbol{a}_N) = \sum_{I=1}^{N} \Psi_c^I(\bar{\boldsymbol{C}}, \mathbb{E}, \boldsymbol{a}_I) = \sum_{I=1}^{N}\sum_{s=1}^{n} \rho_I(\boldsymbol{r}^s)\psi_c^s(\bar{\lambda}_s, E_s), \tag{5}$$

where $\boldsymbol{r}^s \in \mathbb{U}^2$ is the referential unit vector that represents the direction of the s-th chain, and ψ_c^s is the microscopic strain energy of the s-th chain of family I according to the deformation in the direction of $\boldsymbol{r}^s$. In Eqn (5), $E_s = \mathbb{E} \cdot \boldsymbol{r}^s$, $\bar{\lambda}_s = \sqrt{\bar{\boldsymbol{C}} : [\boldsymbol{r}^s \otimes \boldsymbol{r}^s]}$ and $\rho(\boldsymbol{r}^s; \boldsymbol{a}_I)$ is a chain probability distribution function that

will be explained in the next section. For large n, the total isochoric chain energy function for a single family of chains can be expressed as the weighted average of the n contributions, whereby the weight is the chain probability distribution function $\rho_I = \rho_I(\boldsymbol{r}^s)$

$$\Psi_c^I(\bar{\boldsymbol{C}}, \mathbb{E}, \boldsymbol{a}_I) = \langle n\rho_I \psi_c(\bar{\lambda}, E)\rangle. \tag{6}$$

In Eqn (6) $\langle\bullet\rangle$ denotes an averaging operator for scalar quantities and $\bar{\lambda}$ (defined in Eqn (2)) is the macro stretch. The differential area element of the unit sphere $\mathbb{U}^2$ can be expressed in terms of the Eulerian angles as $dA = \sin\Theta d\Theta d\Phi$ which yields the unit sphere's total area if we integrate the surface area, i.e. $A_{\mathbb{U}^2} = \int_0^{\Theta}\int_0^{\Phi} dA = \int_0^{\Theta}\int_0^{\Phi} \sin\Theta d\Theta d\Phi = 4\pi$. We now obtain for the averaging operator by normalising the integral over the unit sphere,

$$\langle n\rho_I \psi_c(\bar{\lambda}, E)\rangle = \frac{1}{4\pi}\int_{\mathbb{U}^2} n\rho_I \psi_c(\bar{\lambda}, E) dA. \tag{7}$$

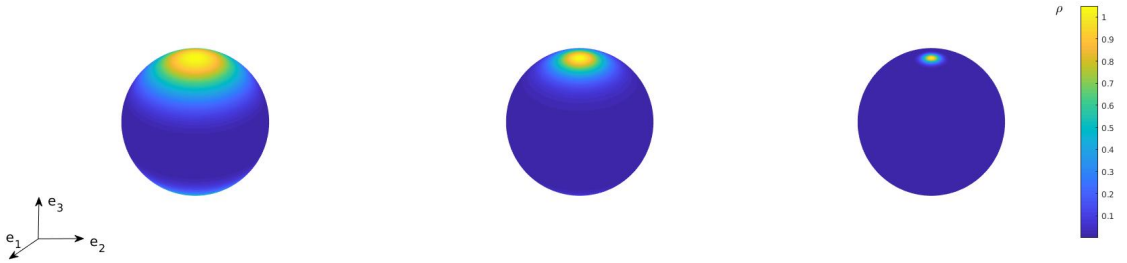

Fig. 3: The von Mises probability distribution function (PDF) presented in Eqn (9) is projected onto the surface of a unit-sphere with respect to various *degree of dispersion* b. (I) $b = 0$, (II) $b = 3.0$, (III) $b = 20.0$. Note that for this particular illustration, the preferential unit vector $\boldsymbol{a}$ is considered in the vertical direction $\boldsymbol{e}_3$. The colour corresponds to the normalised magnitude of the PDF $\rho \in [0, 1]$

In averaging the above formulations, we take an affine assumption for the micro to macro transformation. For a further explanation related to the affine and non-affine kinematics, see Miehe et al. [49], Alastrue et al. [2]. A discrete form of the continuous chain probability distribution function over the unit sphere can be expressed by assuming nid orientation vectors $\{\boldsymbol{r}^s\}_{s=1,\cdots,\text{nid}}$ along with nid weighting factors $\{w^s\}_{s=1,\cdots,\text{nid}}$ as

$$\langle(\bullet)\rangle = \frac{1}{4\pi}\int_{\mathbb{U}^2}(\bullet)dA \approx \sum_{s=1}^{\text{nid}}(\bullet)^s w^s. \tag{8}$$

The micro-sphere based constitutive frameworks obtain popularity in many areas of material modelling due to their simple formulations where complicated tensorial derivations are absent. However, they require high computational costs, see for examples, Miehe et al. [49], Dal et al. [14; 15; 16], Alastrue et al. [2], Ehret et al. [17], Itskov et al., [34], Skacel et al., [64], Pandolfi et al., [54], Nateghi et al. [51].

Now an appropriate probability distribution function (PDF) ρ is required that can accurately capture the effects of the chain distribution. It is assumed that a single chain is symmetrically distributed around the mean direction $\boldsymbol{a}$, i.e., $\rho(\boldsymbol{r};\boldsymbol{a}) = \rho(-\boldsymbol{r};\boldsymbol{a})$ which needs to be incorporated in the PDF. Furthermore, we assume that the chains are rotational symmetrically distributed with respect to the preferred mean direction $\boldsymbol{a}$, i.e., $\rho(\boldsymbol{Q}\cdot\boldsymbol{r};\boldsymbol{a}) = \rho(\boldsymbol{r};\boldsymbol{a})\ \forall \boldsymbol{Q} \in \mathbb{Q}^3_+$ with rotation axis $\boldsymbol{a}$. The normalised π-periodic von Mises PDF has such properties that can represent transversely isotropically distributed chains where it has the form

$$\rho(\chi) = 4\sqrt{\frac{b}{2\pi}}\frac{\exp(b[\cos(2\chi)+1])}{\text{erfi}(\sqrt{2b})}. \tag{9}$$

In Eqn (9), $b \in [0,\infty]$ is a positive concentration parameter that represents a measure of *the degree of anisotropy*, $\text{erfi}(x) = -i\ \text{erf}(x)$ is the imaginary error function, and χ is the angle between unit vectors $\boldsymbol{r}$ and $\boldsymbol{a}$. The angle χ can be calculated by using the scalar product of $\boldsymbol{r}$ and $\boldsymbol{a}$, i.e.

$$\chi = \cos^{-1}(\boldsymbol{a}\cdot\boldsymbol{r}). \tag{10}$$

A three-dimensional presentation of the von Mises PDF is illustrated with respect to different degree of dispersions b in Fig 3 for $\boldsymbol{a} = \boldsymbol{e}_3$, while for a three-dimensional polar plot of the same, see [31].

3 Modelling the curing process in electro-elasticity

During the curing process, a continuous chain cross-linking occurs due to chemical reactions that helps initially scattered monomers to come closer with time to form a cross-linked macromolecular structure. For chemical processes, cross-linkers and other chemical agents are normally added to the system and the results of chemical reactions lead to random networks that eventually yield successive stiffness gaining of the material. Such a continuous stiffness gaining phenomenon, till the end of a curing process, is modelled mathematically under a mechanical load in a series of contributions by Hossain et al. [21; 22; 23; 24]. These frameworks are further extended in the case of particle-filled magneto-active polymers under a magneto-mechanically coupled load, see Hossain et al. [25; 26; 27; 28]. For the curing process in a particle-filled electro-active polymers under an electro-mechanical load, a convolution integral type potential function can be formulated as

$$\begin{aligned}\Phi(\boldsymbol{E},\mathbb{E},t) = \frac{1}{2}\int_0^t \big[\boldsymbol{\mathcal{A}}'(\tau):[\boldsymbol{E}(t)-\boldsymbol{E}(\tau)]\big]:[\boldsymbol{E}(t)-\boldsymbol{E}(\tau)]\ d\tau - \frac{1}{2}\int_0^t \big[\boldsymbol{\mathcal{K}}'(\tau)\cdot[\mathbb{E}(t)-\mathbb{E}(\tau)]\big]\cdot[\mathbb{E}(t)-\mathbb{E}(\tau)]\ d\tau \\ - \int_0^t \big[\boldsymbol{\mathcal{C}}'(\tau)\cdot[\mathbb{E}(t)-\mathbb{E}(\tau)]\big]:[\boldsymbol{E}(t)-\boldsymbol{E}(\tau)]\ d\tau.\end{aligned} \tag{11}$$

In Eqn (11), $\boldsymbol{\mathcal{A}}'(\tau) = d\boldsymbol{\mathcal{A}}(\tau)/d\tau, \boldsymbol{\mathcal{K}}'(\tau) = d\boldsymbol{\mathcal{K}}(\tau)/d\tau$, $\boldsymbol{\mathfrak{C}}'(\tau) = d\boldsymbol{\mathfrak{C}}(\tau)/d\tau$, where $\boldsymbol{E}$ is the Green-Lagrange strain tensor $\boldsymbol{E} := \frac{1}{2}[\boldsymbol{C} - \boldsymbol{I}]$ and $\mathbb{E}$ is the electric field vector in the material configuration. In order to obtain the elasticity tensor $\boldsymbol{\mathcal{A}}$, the piezoelectricity tensor $\boldsymbol{\mathfrak{C}}$, and the dielectricity tensor $\boldsymbol{\mathcal{K}}$ in the material configuration, an energy function $\Omega(t)$, similar to the one commonly used for a fully-cured electro-elastic polymer modelling, is required. With time-dependent or degree of cure-dependent parameters appearing in the energy function, the above mentioned stiffness moduli are defined as

$$\boldsymbol{\mathcal{A}}(\boldsymbol{E}, \mathbb{E}, t) = \frac{\partial^2 \Omega(t)}{\partial \boldsymbol{E} \otimes \partial \boldsymbol{E}}, \quad \boldsymbol{\mathfrak{C}}(\boldsymbol{E}, \mathbb{E}, t) = -\frac{\partial^2 \Omega(t)}{\partial \boldsymbol{E} \otimes \partial \mathbb{E}}, \quad \boldsymbol{\mathcal{K}}(\boldsymbol{E}, \mathbb{E}, t) = -\frac{\partial^2 \Omega(t)}{\partial \mathbb{E} \otimes \partial \mathbb{E}}. \tag{12}$$

To guarantee thermodynamically consistent formulations, the second law of thermodynamics in the form of the so-called Clausius-Duhem inequality needs to be fulfilled. For an isothermal process in the case of an electro-mechanical coupled problem, this law can be written as

$$\boldsymbol{S} : \dot{\boldsymbol{E}} - \mathbb{D} \cdot \dot{\mathbb{E}} - \dot{\Phi} \geq 0, \tag{13}$$

where $\boldsymbol{S}$, $\mathbb{D}$ and Φ are the total second Piola-Kirchhoff stress tensor, the electric displacement vector in the material configuration and the potential function Φ proposed in Eqn (11), respectively. When the time derivative of the potential function Φ is inserted in the above form of the dissipation inequality, i.e. Eqn (13) and after some rigorous calculations, we obtain more precise and explicit relations between stress-strain and electric displacement-electric field as

$$\dot{\boldsymbol{S}}(\boldsymbol{E}, \mathbb{E}, t) = \boldsymbol{\mathcal{A}} : \dot{\boldsymbol{E}} - \boldsymbol{\mathfrak{C}} \cdot \dot{\mathbb{E}} = \frac{1}{2}\boldsymbol{\mathcal{A}} : \dot{\boldsymbol{C}} - \boldsymbol{\mathfrak{C}} \cdot \dot{\mathbb{E}}, \tag{14}$$

$$\dot{\mathbb{D}}(\boldsymbol{E}, \mathbb{E}, t) = \boldsymbol{\mathfrak{C}}^t : \dot{\boldsymbol{E}} + \boldsymbol{\mathcal{K}} \cdot \dot{\mathbb{E}} = \frac{1}{2}\boldsymbol{\mathfrak{C}}^t : \dot{\boldsymbol{C}} + \boldsymbol{\mathcal{K}} \cdot \dot{\mathbb{E}}, \tag{15}$$

where $\boldsymbol{\mathfrak{C}}^t$ is the transpose of the third order coupling stiffness tensor $\boldsymbol{\mathfrak{C}}$. Note that a detailed and step by step derivations of the equations (14) and (15) are omitted here since a similar framework in the case of magneto-elasticity is derived in Hossain et al. [25]. Using an Euler-backward type implicit integrator, we can obtain the updates for the algorithmic stress tensor and the electric displacement vector

$$\boldsymbol{S}^{n+1} = \boldsymbol{S}^n + \frac{1}{2}\boldsymbol{\mathcal{A}}^{n+1} : [\boldsymbol{C}^{n+1} - \boldsymbol{C}^n] - \boldsymbol{\mathfrak{C}}^{n+1} \cdot [\mathbb{E}^{n+1} - \mathbb{E}^n], \tag{16}$$

$$\mathbb{D}^{n+1} = \mathbb{D}^n + \frac{1}{2}\boldsymbol{\mathfrak{C}}^{t,n+1} : [\boldsymbol{C}^{n+1} - \boldsymbol{C}^n] + \boldsymbol{\mathcal{K}}^{n+1} \cdot [\mathbb{E}^{n+1} - \mathbb{E}^n]. \tag{17}$$

In Eqns (16) and (17), $[\bullet]^n = [\bullet](t_n)$, $t_{n+1} = t_n + \Delta t$ and Δt is a time step.

4 Modelling curing shrinkage in composite EAPs

During the process of curing, initial monomers come closer to form new chemical bonds and then gradually form a chain-like macromolecular structure with the help of cross-linkers and other chemical agents. Such successive cross-linking of polymer chains will lead to more dense packing situation compared to an uncured monomeric solution. As a result, one important but undesirable property of polymers is a volume reduction that is known as the curing shrinkage in the curing process [41]. To capture such a phenomenon in finite strain settings, a multiplicative decomposition-type modelling approach has originally been formulated by Lion and Höfer [44] in the case of a purely mechanical curing where the deformation gradient is decomposed into two parts: a stress producing mechanical part $\boldsymbol{F}_m$ and a volume reducing shrinkage part $\boldsymbol{F}_s$, i.e.,

$$\boldsymbol{F} = \boldsymbol{F}_m \boldsymbol{F}_s \quad \text{with} \quad \boldsymbol{F}_s = [1 + \alpha s]^{1/3} \boldsymbol{I}, \tag{18}$$

where $\alpha \in [0, 1]$ denotes the so-called *degree of cure*, $s \leq 0$ is a parameter that gauges the magnitude of the volume shrinkage, and $\boldsymbol{I}$ is a second order unit tensor. Note that the above formulation can only be applied when a same amount of volume shrinkage occurs in all directions which is the case ideal for an unfilled polymer. For the electro-mechanically coupled curing in EAP composites, we assume that the presence of an electric field affects the overall curing process in two ways which will be explained in the following.

Coupled curing shrinkage: Effect I

The first assertion is that the amount and nature of the curing shrinkage under an electric field is not only dependent on the curing time or the degree of cure but also on the magnitude and duration of exposure of the applied electric field $\mathbb{E}$. Hence the shrinkage part of the deformation gradient in (18) is modified to

$$\boldsymbol{F}_s = [1 + \alpha s\{\alpha, \mathbb{E}\}]^{1/3} \boldsymbol{I}. \tag{19}$$

Recently, a similar approach has been formulated for the case of magneto-mechanically coupled curing by Hossain et al. [25; 26; 27; 28]. To account the overall influence of an electric field on the curing process, we define a new parameter 'degree of exposure' e_E as

$$e_E = \int_0^t f\big(\alpha(\tau)\big)\, |\mathbb{E}(\tau)|\, d\tau, \quad \text{with,} \quad f(\alpha) = 1 - H(\alpha - 1), \tag{20}$$

where H is the Heaviside function and $|\mathbb{E}(\tau)|$ is the magnitude of the applied electric field. The parameter e_E incorporates a duration time of the applied electric field that is activated during the curing process. In order to include the fluctuating influence of an electric field to the constitutive model, the function $f(\alpha)$ is introduced. Two extreme values of exposure are defined as $0 < e_{E1} < e_{E2}$ which simply imply that when the lower

value of the degree of exposure e_E crosses the threshold e_{E1} it starts increasing the value of the shrinkage parameter s from an initial value of s_1. When it reaches the upper threshold value e_{E2}, the maximum possible value of shrinkage $s = s_2$ is reached and the evolution of s remains unchanged. All these information can be incorporated once the evolution of s can be expressed by the following functional form

$$s = \frac{s_1 + s_2}{2} + \frac{s_2 - s_1}{2} \tanh\left(\xi\left[e_E - \frac{1}{2}[e_{E1} + e_{E2}]\right]\right), \tag{21}$$

where ξ is a scaling constant. Evolutions of the shrinkage parameter s with respect to the degree of exposure e and curing time for a scaling factor $\xi = 1$ are depicted in Fig 4.

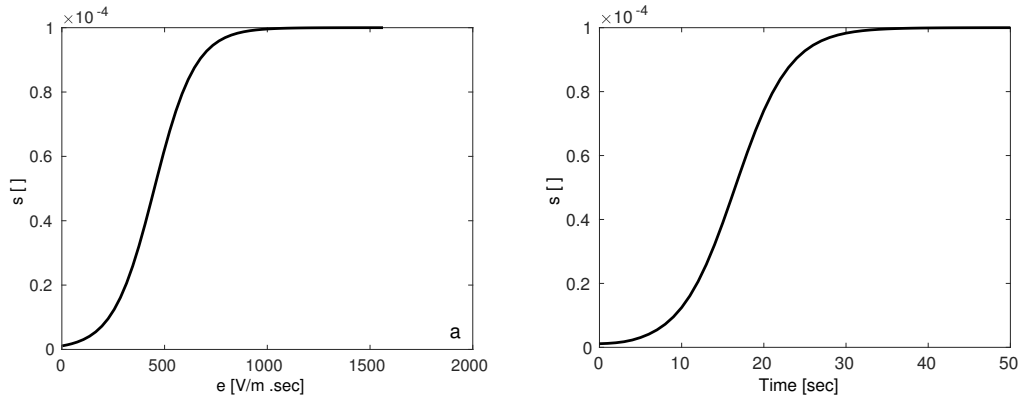

Fig. 4: Evolutions of the shrinkage parameter s with respect to (left) the degree of exposure e, (right) curing time for a scaling factor $\xi = 1$

Coupled curing shrinkage: Effect II

For an isotropic curing process, the same amount of volume shrinkage can occur in all directions. However, for an anisotropic curing process, which is the case for the curing under an electric field, the amount of the volume shrinkage is not the same in all directions. It can be easily predicted that a less amount of volume shrinkage will occur in the direction of the particles alignment due to the action of an electric field. The directional-dependency (anisotropy) with a chain dispersion will also influence the total amount of shrinkage. In the case of particle-filled EAPs when the curing occurs in an electric field, high conductive particles are aligned in a preferred direction $\boldsymbol{a}$. Hence the reformulated equation in (19) will be transformed to

$$\boldsymbol{F}_s = [1 + \alpha s\{\alpha, \mathbb{E}\}]^{1/3} [\boldsymbol{I} - \beta \boldsymbol{a} \otimes \boldsymbol{a}] + \beta \boldsymbol{a} \otimes \boldsymbol{a}, \tag{22}$$

where β is a scaling parameter $0 < \beta < 1$ that can be related to the degree of dispersion b. For a particular preferred (mean) direction $\boldsymbol{a}$, the scaling factor β can be determined by

$$\beta = \frac{\sum_{s=1}^{\text{nid}} \rho(\boldsymbol{r}^s, \boldsymbol{a})}{\sum_{s=1}^{\text{nid}} \rho_{\text{max}}(\boldsymbol{r}^s, \boldsymbol{a})}, \tag{23}$$

where $\rho_{\text{max}}(\boldsymbol{r}^s; \boldsymbol{a})$ is the ultimate value of the PDF evaluated at the maximum value of b, i.e., $b = 20$. Once formulations of the shrinkage part of the deformation gradient $\boldsymbol{F}_s$ is determined, the multiplicative decomposition of the deformation gradient yields the cure-dependent right Cauchy-Green tensor and the electro-mechanical stress tensor as

$$\boldsymbol{C}_m = \boldsymbol{F}_m^t \boldsymbol{F}_m = \boldsymbol{F}_s^{-2} \boldsymbol{C}, \qquad \boldsymbol{S} = \boldsymbol{F}_s^{-1} \boldsymbol{S}_m \boldsymbol{F}_s^{-t}. \tag{24}$$

5 A specified energy function

For the calculation of the three stiffness moduli $\mathcal{A}, \mathfrak{C}, \mathcal{K}$ formulated in Eqns (14) and (15), an electro-mechanically coupled energy function is required. In this section, a specific energy function will be formulated that will take into account the dispersion anisotropy in electro-active polymers. If the so-called free-space term contribution outside the matter is included, the total energy function reads as

$$\Omega(\boldsymbol{F}, \mathbb{E}, \boldsymbol{a}) = \Psi(\boldsymbol{F}, \mathbb{E}, \boldsymbol{a}) + E_0(\boldsymbol{F}, \mathbb{E}) \tag{25}$$

which can be further decomposed into

$$\Omega(\boldsymbol{F}, \mathbb{E}, \boldsymbol{a}) = \Psi_{\text{vol}}(J) + \Psi_{\text{iso}}^{\text{isp}}(\bar{\boldsymbol{C}}, \mathbb{E}) + \Psi_{\text{iso}}^{\text{ani}}(\bar{\boldsymbol{C}}, \mathbb{E}, \boldsymbol{a}_1, \cdots, \boldsymbol{a}_N) + E_0(\boldsymbol{F}, \mathbb{E}). \tag{26}$$

The vacuum permittivity associated with $E_0(\boldsymbol{F}, \mathbb{E})$ has insignificant contribution in the overall calculations. Hence it will be neglected in this contribution as in [68; 46], i.e. $\Omega(\boldsymbol{F}, \mathbb{E}, \boldsymbol{a}) \approx \Psi(\boldsymbol{F}, \mathbb{E}, \boldsymbol{a})$ is assumed in the subsequent calculations. To obtain a complete expression for the energy function in Eqn (4), appropriate choices for the isotropic energy function $\Psi_{\text{iso}}^{\text{isp}}$ as well as for the anisotropic energy function $\Psi_{\text{iso}}^{\text{ani}}$ need to be determined. The Neo-Hookean type electro-mechanically coupled strain energy function is often used in electro-elasticity. Therefore, as a starting point in the modelling of curing process under an electro-mechanically coupled load, we assume a Neo-Hookean-like material as follows

$$\Psi_{\text{iso}}^{\text{isp}}(\bar{\boldsymbol{C}}, \mathbb{E}) = \frac{1}{2}\mu \left[\bar{I}_1 - 3\right] + n_e[\mathbb{E} \otimes \mathbb{E}] : \bar{\boldsymbol{C}}^{-1} + m_e[\mathbb{E} \otimes \mathbb{E}] : \boldsymbol{I} \tag{27}$$

where m_e and n_e are electrostrictive coupling coefficients. Similar to the Neo-Hookean structure of the isotropic part of the macroscopic energy appearing in Eqn (27), a Neo-Hookean type free energy function for a single chain is chosen. After performing the averaging operation on the unit sphere including scaling by the von Mises PDF ρ for a single family of chains, we obtain the macroscopic form of the anisotropic energy function as

$$\Psi_{\text{iso}}^{\text{ani}}(\bar{\boldsymbol{C}}, \mathbb{E}, \boldsymbol{a}) \approx \sum_{s=1}^{\text{nid}} \rho^s \, \psi_c^s \, w^s = \sum_{s=1}^{\text{nid}} \rho^s \underbrace{\left[\frac{1}{2}\tilde{\mu}[\bar{\lambda}_s^2 - 1] + c_1 \bar{\lambda}_s^2 E_s^2 + c_2 E_s^2\right]}_{\psi_c^s} w^s \tag{28}$$

where $\tilde{\mu}$, c_1 and c_2 are the chain shear modulus and the coupling parameters, respectively, in the micro-sphere energy function ψ_c^s. Finally, after combining the isotropic coupled function in (27) and the anisotropic coupled function in (28), a complete form of the compressible energy function becomes

$$\begin{aligned}\Psi(\boldsymbol{C}, \mathbb{E}, \boldsymbol{a}) = \frac{\kappa}{2}[\ln J]^2 - \mu \ln J + \frac{1}{2}\mu\,[I_1 - 3] + n_e[\mathbb{E} \otimes \mathbb{E}] : \boldsymbol{C}^{-1} + m_e[\mathbb{E} \otimes \mathbb{E}] : \boldsymbol{I} \\ + \sum_{s=1}^{\text{nid}} \rho^s \left[\frac{1}{2}\tilde{\mu}[\lambda_s^2 - 1] + c_1 \lambda_s^2 E_s^2 + c_2 E_s^2\right] w^s.\end{aligned} \tag{29}$$

Note that this particular form of compressible Neo-Hooke energy function for the mechanical part appearing in the first part of the total coupled energy has shortcomings, e.g. the term $\kappa[\ln J]^2$ does not satisfy the so-called growth conditions and the convexity requirements of elasticity. In order to facilitate for a closed form solution in the subsequent part, we have chosen this particular form of Neo-Hooke energy function. However, our modelling framework described in the previous sections is a generalised one that can fit to any advanced form of energy function. For given values of the deformation gradient $\boldsymbol{F}$ and the electric field vector $\mathbb{E}$, the stiffness moduli tensors $\boldsymbol{\mathcal{A}}, \boldsymbol{\mathcal{C}}, \boldsymbol{\mathcal{K}}$ need to be derived from the energy function presented in Eqn (29). Thus, the elasticity tensor is given as

$$\begin{aligned}\boldsymbol{\mathcal{A}} &= \frac{\partial^2 \Psi}{\partial \boldsymbol{E} \otimes \partial \boldsymbol{E}} \\ &= \kappa\, \boldsymbol{C}^{-1} \otimes \boldsymbol{C}^{-1} - 2\,[\mu - \kappa \ln J]\, \frac{\partial \boldsymbol{C}^{-1}}{\partial \boldsymbol{C}} + 4 n_e\, [\mathbb{E} \otimes \mathbb{E}] : \frac{\partial}{\partial \boldsymbol{C}}\Big(\frac{\partial \boldsymbol{C}^{-1}}{\partial \boldsymbol{C}}\Big) \\ &+ \sum_{s=1}^{\text{nid}} \rho^s \bar{\lambda}_s^{-2} \left[\frac{\partial^2 \psi_c^s}{\partial \bar{\lambda}_s \partial \bar{\lambda}_s} - \bar{\lambda}_s^{-1} \frac{\partial \psi_c^s}{\partial \bar{\lambda}_s}\right] \boldsymbol{r}^s \otimes \boldsymbol{r}^s \otimes \boldsymbol{r}^s \otimes \boldsymbol{r}^s w^s.\end{aligned} \tag{30}$$

The tensor derivative of $\frac{\partial \boldsymbol{C}^{-1}}{\partial \boldsymbol{C}}$ can be expressed as component-wise, i.e., $\Big(\frac{\partial \boldsymbol{C}^{-1}}{\partial \boldsymbol{C}}\Big)_{ijkl} = -\frac{1}{2}\Big[C_{ik}^{-1} C_{jl}^{-1} + C_{il}^{-1} C_{jk}^{-1}\Big]$. Furthermore, $\frac{\partial}{\partial \boldsymbol{C}}\Big(\frac{\partial \boldsymbol{C}^{-1}}{\partial \boldsymbol{C}}\Big)$ is also given in component-wise: $-\frac{1}{2}\frac{\partial\left(C_{ik}^{-1} C_{jl}^{-1} + C_{il}^{-1} C_{jk}^{-1}\right)}{\partial C_{pq}} = \frac{1}{4}\Big[C_{ip}^{-1} C_{kq}^{-1} C_{jl}^{-1} + C_{iq}^{-1} C_{kp}^{-1} C_{jl}^{-1} + C_{ik}^{-1} C_{jp}^{-1} C_{lq}^{-1} + C_{ik}^{-1} C_{jq}^{-1} C_{lp}^{-1} + C_{ip}^{-1} C_{lq}^{-1} C_{jk}^{-1} + C_{iq}^{-1} C_{lp}^{-1} C_{jk}^{-1} + C_{il}^{-1} C_{jp}^{-1} C_{kq}^{-1} + C_{il}^{-1} C_{jq}^{-1} C_{kp}^{-1}\Big]$.

The third-order so-called piezoelectric tensor is

$$\mathfrak{C} = -\frac{\partial^2 \Psi}{\partial \boldsymbol{E} \otimes \partial \mathbb{E}} = -2\frac{\partial^2 \Psi}{\partial \boldsymbol{C} \otimes \partial \mathbb{E}} = -4n_e \mathbb{E} \cdot \frac{\partial \boldsymbol{C}^{-1}}{\partial \boldsymbol{C}} - \sum_{s=1}^{\text{nid}} \rho^s \bar{\lambda}_s^{-1} \frac{\partial^2 \psi_c^s}{\partial E_s \partial \bar{\lambda}_s} \boldsymbol{r}^s \otimes \boldsymbol{r}^s \otimes \boldsymbol{r}^s w^s, \tag{31}$$

while the dielectric tensor can be obtained as

$$\mathfrak{K} = -\frac{\partial^2 \Psi}{\partial \mathbb{E} \otimes \partial \mathbb{E}} = -2m_e \boldsymbol{I} - 2n_e \boldsymbol{C}^{-1} + \sum_{s=1}^{\text{nid}} \rho^s \frac{\partial^2 \psi_c^s}{\partial E_s \partial E_s} \boldsymbol{r}^s \otimes \boldsymbol{r}^s w^s. \tag{32}$$

6 Numerical examples

In this section, the capability of the cure-dependent model developed in the sections above will be demonstrated with the help of several benchmark examples. For a certain deformation and an electric field, updates of the total stress and the electric displacement are calculated according to Eqns (16) and (17), respectively. The equations are discretised using an Euler-backward type implicit integrator. For incorporations of the stiffness gain and other observed phenomena during the curing, relevant parameters appearing in the model are to be evolved with time. The free energy function expressed in Eqn (29) has several material parameters where the shear modulus is a key material parameter for the realisation of the stiffness gain during the curing process. For coupled electro-mechanical parameters, we can take similar mathematical formulations as in the case of mechanical material parameters, e.g. shear modulus. One of the easiest formats for the evolution of these parameters is an exponential saturation function. Therefore, the evolutions of shear modulus μ and electro-mechanical coupled parameters, namely n_e, are considered as

$$\mu(t) = \mu_0 + [\mu_\infty - \mu_0]\left[1 - \exp(-\kappa_\mu t)\right], n_e(t) = n_{e0} + [n_{e\infty} - n_{e0}]\left[1 - \exp(-\kappa_{ne} t)\right], \tag{33}$$

where μ_0, n_{e0} and $\mu_\infty, n_{e\infty}$ are initial and final cut-off values of a particular material parameter, respectively. In Eqn (33) κ_μ, κ_{ne} are curvature parameters. All other parameters appearing in the model are assumed to be insensitive to the curing process. Note that a numerical integration schemed is required to perform the integration over the unit sphere, e.g. in Eqn (30). Several angular integration procedures are proposed and their comparisons are critically discussed in the literature for purely mechanical loadings, see [17; 34; 71]. Since the aim of the current contribution is not to focus on the integration schemes, we stick to use the 64-integration point proposed by Womersley [71] due to its excellent performance which is recently analysed in the case of fully cured electro-elastic modelling in Hossain and Steinmann [31].

6.1 Uniaxial tests : Pull-hold-pull load

At first, several numerical examples with uniaxial type loading are demonstrated to ensure that the developed constitutive framework can predict stiffness gaining during curing processes under an electro-mechanically coupled load. In the case of a uniaxial tension test, the specimen is elongated only in one direction, i. e. $\lambda_1 = \lambda$, while the other two lateral directions are free to move. Here, the deformation gradient is expressed as $\boldsymbol{F} = \lambda \boldsymbol{e}_1 \otimes \boldsymbol{e}_1 + \lambda_2 \boldsymbol{e}_2 \otimes \boldsymbol{e}_2 + \lambda_2 \boldsymbol{e}_3 \otimes \boldsymbol{e}_3$ while the electric field vector is $\mathbb{E} \equiv [E_1, 0, 0]^t$, where λ is the stretch in the load direction and E_1 is the electric field component in the same direction. Due to the compressibility assumption of the constitutive model under consideration, we need to establish a relation between λ_1 and λ_2 ($\lambda_2 = \lambda_3$, in the case of a symmetric deformation). For a compressible Neo-Hookean type material which is the case expressed in Eqn (29), we establish an analytical relation between λ_1 and λ_2 (= λ_3) in the case of a simple uniaxial deformation. Detailed descriptions of such a relation are skipped here due to its length expressions. However, a similar procedure is illustrated in our previous works, see Hossain et al. [26; 27]. Note that since the elongation is only in one direction, both lateral components of the nominal stress P=diag$\{P_{11}; P_{22}; P_{33}\}$, i.e. P_{22} and P_{33} are zero and only component P_{11} needs to be determined. For the numerical examples presented here, few material parameters used are as follows

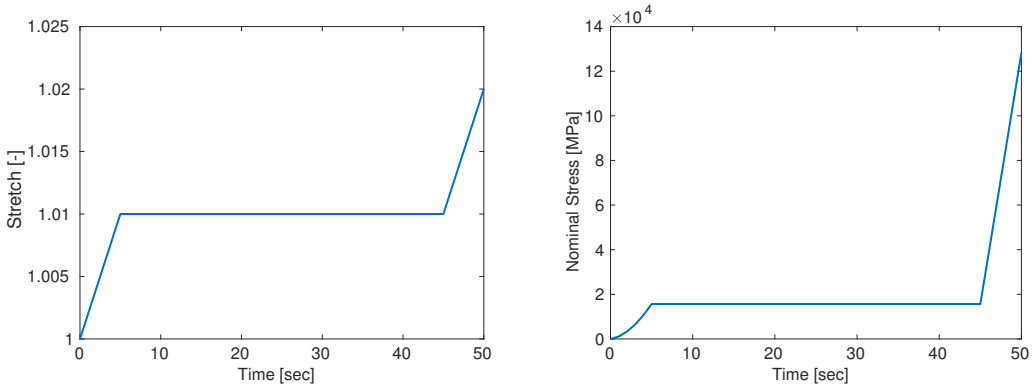

Fig. 5: (Left) A three-phase *pull-hold-pull* pure mechanical load applied in 50 sec curing time, (Right) Stress response during the curing process under a mechanical load

$$\mu_{in} = 1.0 \times 10^{-11}\,\text{MPa}, \quad \mu_{\infty} = 5.0 \times 10^{6}\,\text{MPa}, \quad \kappa_{\mu} = 0.0825\ s^{-1}$$
$$n_{e0} = -1.0 \times 10^{-11}\ \text{N/V}^2, \quad n_{e\infty} = -6\ \text{N/V}^2, \quad \kappa_{ne} = 0.0825\ s^{-1}. \tag{34}$$

Note that a similar set of material parameters is used by Saxena et al. [62] in the modelling of fully-cured electro-active polymers. During the development of the cure-dependent electro-mechanically coupled model

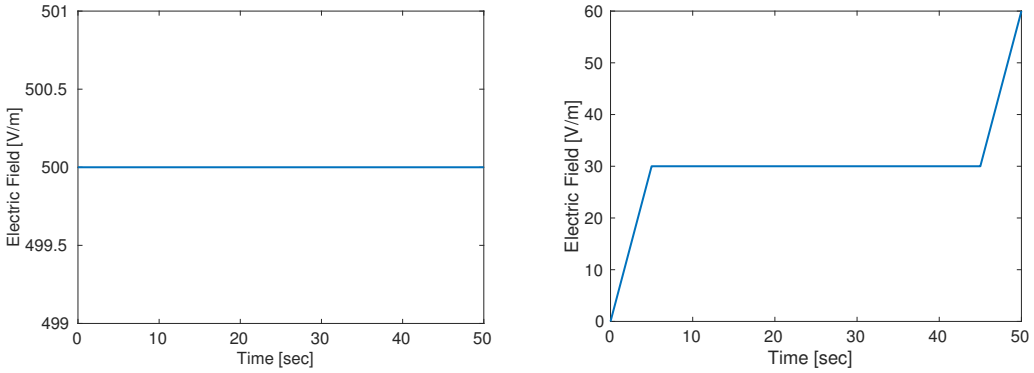

Fig. 6: (Left) A constant amount of electric field applied throughout the curing time, (Right) A three-phase electric load similar to the three phase mechanical load

explained in Sections 3 and 4, two main observations are taken into account, i.e. the stiffness gain due to the continuous chain cross-linking with an advancement of the curing process and the chain formation should be stress-free, see Gillen [20], Adolf [1]. Moreover, an electric field further affects the material stiffness [10]. To demonstrate the incorporation of all three major assumptions within the constitutive framework, a three phase *pull-hold-pull* electro-mechanically coupled load is applied. At first, the purely mechanical part of the model formulated in Eqn (16) will be verified whether it can capture stiffness gaining as well as it can also capture the effects of chain dispersions during the curing process. For this, a three phase pure mechanical load is applied as in Fig 5 (left). The results for this loading is presented correspondingly in Fig 5 (right). It is clear from the figure that for a purely mechanical *pull-hold-pull* load, the stress development is larger in the third load phase compared to the first phase while there is no stress increment during the load holding period of 6-45 sec.

Now the influence of a constant amount of electric field on the stress response during the three phase pull-hold-pull loading will be checked. As mentioned earlier, for a constant amount of electric field, cf Fig 6 (left), along with a mechanical load during the entire curing time, the overall stress response will increase in contrast to the purely mechanical loading, see Fig 7 (left). If the magnitude of the electric field is increased, the total stress is also elevated at a higher value. To illustrate the stiffness gain under an electro-mechanical coupled load, the total coupled nominal stress is plotted over the mechanical stretch in Fig 7 (right).

In order to demonstrate combined effects of electro-mechanical coupled loads and the chain dispersions, we now apply a three phase mechanical, cf. Fig (5, left) and a three-phase electric loading, cf. Fig (6, right). For this combined loading, the total nominal stress over the stretch is depicted in Fig (8, left). It is again clear that an electric field produces additional stress in addition to the mechanical stress. Moreover, this total stress is increasing with a decreasing trend of the dispersion, characterised by a higher value of the dispersion param-

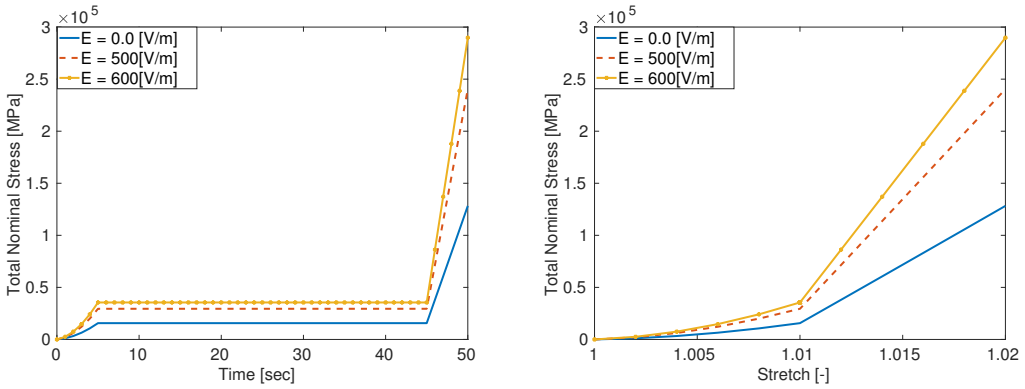

Fig. 7: Effects of a constant amount of electric field: (Left) Electric field affects the total coupled stress and it increases with the increase of the field, (Right) The effects are more vivid when the coupled stress is plotted over the mechanical stretch

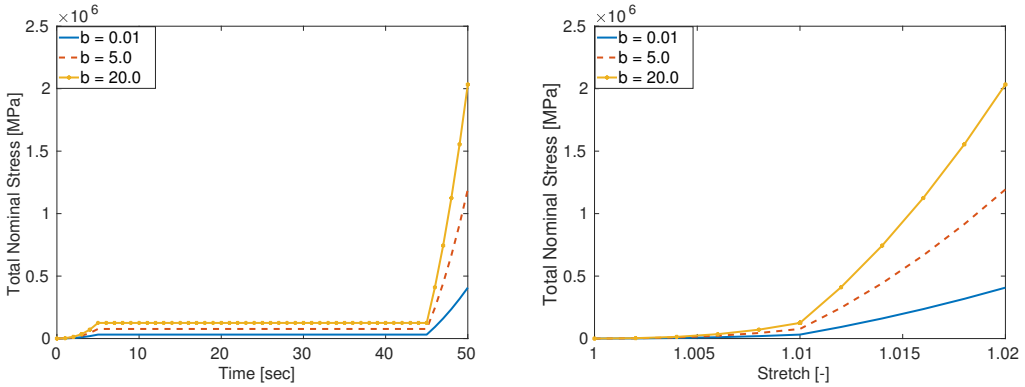

Fig. 8: Effects of the chain dispersion on the total coupled stress : (Left) The total coupled stress is increased with the alignment of particles in the load direction characterised by the dispersion parameter b, (Right) Total stress is plotted over the mechanical stretch to observe the effects of chain dispersions

eter b. Similar to the three-phase purely mechanical load, the stress development in the electro-mechanically coupled case is much more in the third load phase compared to the first phase while there is no stress increment during the load holding period of 6-45 sec. The total electro-mechanical stiffness gain is more vivid when the total coupled stress is plotted over the mechanical stretch, see Fig (8, right).

At this stage, evolutions of the electric displacement during the curing process will be illustrated. For a three-phase electro-mechanically coupled loading, the corresponding electric displacement is plotted in Fig (9, left). It is clear from the figure that the electric displacement is greater in the second loading phase compared to the first phase. However, the increments of the electric displacement in the second load step are not qualitatively as large as the total stress. The reason is, for the electric part of the energy function, we assume that only the coupling parameter n_e is evolving with respect to the curing process. There is no temporal change of the

electric parameter m_e during the process. However, this assumption is flexible that can easily be modified as soon as we will have enough experimental data. Now, the influence of the dispersion phenomenon on the electric displacement is tracked with the model. As expected, for a greater value of the degree of dispersion characterised via b, filler particles will align in the direction of the applied field that results in a larger electric displacement. In order to illustrate the results in a more explicit manner, we plot the electric displacement over the electric field that represents the electric stiffness gain during the curing process, cf. Fig (9, right).

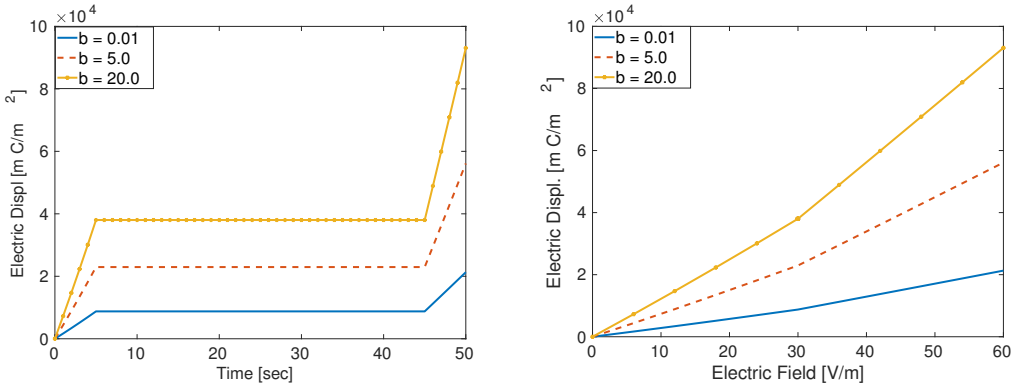

Fig. 9: Evolutions of electric displacements during the curing process: (Left) Response of the electric displacement over the curing time, (Right) Electric displacement is increasing with respect to the chain alignment in the applied field direction

6.2 Curing shrinkage under a coupled load

In this section, the effects of coupled load as well as the chain dispersions will be illustrated on the curing-induced shrinkage behaviours. For this, the multiplicative decomposition type shrinkage model systematically presented in Section (4) will be utilised. In addition to the material parameter set listed in Eqn (33), some more parameters required for the numerical examples are presented here. The evolution for the degree of cure α required in Section (4), e.g., in Eqn (19) is considered as an exponential saturation function similar to Eqn (33), i.e. $\alpha(t) = \alpha_0 + [\alpha_\infty - \alpha_0]\,[1 - \exp(-\kappa_\alpha t)]$. For the initial and the final cut-off values of the degree of cure, i.e. α_0 and α_∞ are considered as 1.0×10^{-8} and 1.0, respectively. For a fifty second curing time, the curvature parameter κ_α, required in the above formulation, is taken as $0.0825\ s^{-1}$. In order to see the effects of an electric field on the nature and magnitude of the shrinkage-induced stress, at first, it is assumed that the shrinkage parameter s does not depend on the electric load $\mathbb{E}$, i.e. there is no direct coupling between s and $\mathbb{E}$. In this case, the curing-induced volume reduction parameter is taken as $s = -1.0 \times 10^{-4}$. A three-phase pure mechanical load enhanced by a three-phase electric field applied throughout the curing time is utilized. The stress evolution by the three-phase *pull-hold-pull* electro-mechanically coupled load without a

curing shrinkage model is plotted with a solid line in Fig (10, left). In the same figure, the stress response for an isotropic curing (Eqn., 18) is plotted (dashed line) while the effect of an anisotropic curing (Eqn., 22) is depicted with a solid-stared line. For the latter case, the anisotropic scaling parameter β is taken as a dispersion-independent constant, e.g. $\beta = 0.3$. It is clear from figure (10, left) that the amount of curing-induced shrinkage in the anisotropic case is less than the isotropic shrinkage since the particle alignments restrict the shrinkage in the applied electric field direction. Furthermore, for both isotropic and anisotropic cases, the shrinkage-induced total stress is higher than the no-shrinkage total coupled stress in the plateau region (6-45 sec) since both the electro-mechanical load and the shrinkage-generated load contribute to the stress development in this region.

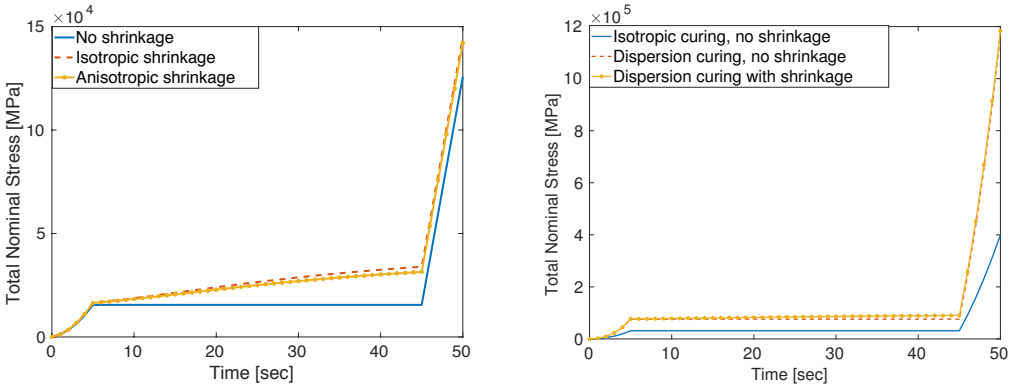

Fig. 10: Effects of the curing shrinkage on the stress evolution with a three-phase coupled loading: (Left) Comparison between isotropic and transversely isotropic curing shrinkages, (Right) Comparison shows that the dispersion of the chains affect the total amount of shrinkage

Now we want to demonstrate how the chain dispersion affects the shrinkage-induced stress generation during the curing process. For this, in contrast to the previous case, the anisotropic scaling parameter β will be related to the degree of dispersion b via Eqn (23). The mathematical formulations presented in Eqn (23) establish that for a smaller value of b, that corresponds to a highly chain-dispersed situation, β gets a smaller value and vice-versa. A strict alignment of the chains in the direction of the applied electric field yields less shrinkage-induced stress, see Fig (10, right). Similar to the previous case, a three-phase electric load is applied along with the three phase mechanical load. For the figure (10, right), a medium value of $b = 5$ is used to calculate the anisotropic parameter β using Eqn (23).

7 Conclusion and outlook

Within this contribution a three-dimensional electro-elastic constitutive framework that can model the stiffness gaining during the curing process undergoing finite deformations is presented. We propose the cure-dependent

electro-elastic model in the spirit of a dispersion-type anisotropy since, according to the recent experimental data presented in the literature, a chain-like micro-structure is formed by filler particles when EAP composites are being cured under an electric field. Moreover, to capture the volume shrinkage, a directional-dependent shrinkage model is formulated that takes into account the dispersion anisotropy. Some well-known benchmark numerical examples show that all relevant phenomena can be envisaged in an environment where a curing process occurs under an electro-mechanically coupled load. To simulate real life examples, these modelling frameworks will be implemented in an electro-mechanically coupled finite element code. Furthermore, the temperature evolution is a common phenomenon during the curing process. Hence a thermo-electro-elastic extension of the framework is essential that will be our current area of study. In the near future, there is a plan to validate the model with a real experimental data.

References

1. Adolf D B, Martin J E, Chambers R S, Burchett S N, Guess T N (1998), Stresses during thermoset cure, Journal of Materials Research 13:530-550
2. Alastrue V, Martinez M, Doblare M, Menzel M, Anisotropic micro-sphere-based finite elasticity applied to blood vessel modeling, International Journal of Mechanics and Physics of Solids, 57:178-203, 2009
3. Ask A, Menzel A, Ristinma M, Phenomenological modeling of viscous electrostrictive polymers, International Journal of Non-Linear Mechanics, 47(2):156-165, 2012
4. Bazant Z P, Oh B H, Efficient numerical integration on the surface of a sphere, Z. Angew. Math. Mech.66:37-49, 1986
5. Büschel A, Klinkel S and Wagner W, Dielectric elastomers- Numerical modeling of nonlinear visco-elasticity, International Journal of Numerical Methods in Engineering 93:834-856, 2013
6. Bustamante B, Transversely isotropic nonlinear electro-active elastomers, Acta Mechanica, 206(3-4):237-259, 2009
7. Carpi F, Rossi D D, Improvement of electromechanical actuating performances of a silicone dielectric elastomer by dispersion of titaniun dioxide powder, IEEE Trans Dielectr Electr Insul, 12:835-843, 2005
8. Carpi F, Gallone G, Galantini F, Rossi D D, Silicone-poly(hexylthiophene) blends as elastomers with enhanced electromechanical transduction properties, Adv Funct Mater, 18:235-241, 2008
9. Cortes D H, Lake S P, Kadlowec J A, Soslowsky L J, Elliot D M, Characterizing the mechanical contribution of fiber angular distribution in connective tissue: comparison of two modeling approaches, Biomech Model Mechanobiol, 9:651-658, 2010
10. Dorfmann A and Ogden R W, Nonlinear electroelasticity, Acta Mechanica, 174(3):167-183, 2005
11. Dorfmann L, Ogden R W, Nonlinear electroelasticity : material properties, continuum theory and applications. Proceedings of the Royal Society/ A, 473, 20170311, 2017
12. Diaconu I, Dorohoi D O and Ciobanu C, Eletromechanical response of polyurethane films with different thickness, Romanian Journal of Physics, 53(1-2):91-97, 2008
13. Dang Z M, Yuan J K, Zha J W, Zhou T, Li S T, Hu G H, Fundamentals, processes and applications of high-permittivity polymer-matrix composites, Prog Mater Sci, 57:660-723,2012
14. Dal H, Zopf C, Kaliske M, Micro-sphere based viscoplastic constitutive model for uncured green rubber, International Journal of Solids and Structures, 132?133: 201-217, 2018

15. Dal H, Kaliske M, A micro-continuum-mechanical material model for failure of rubber-like materials: Application to ageing-induced fracturing, International Journal of Mechanics and Physics of Solids, 57(8): 1340-1356, 2009
16. Dal H, Cansiz B, Miehe C, , A three?scale compressible microsphere model for hyperelastic materials, International Journal of Numerical Methods in Engineering, 116:412-433, 2018
17. Ehret A E, Itskov M, Schmid H, Numerical integration on the sphere and its effect on the material symmetry of constitutive equations- a comparative study, International Journal of Numerical Methods in Engineering, 81:189-206, 2010
18. Fliege J, Maier U, The distribution of points on the sphere and corresponding cubature formulae. IMA Journal of Numerical Analysis 19(2):317-334, 1999
19. Gallone G, Carpi F, Rossi D D, Levita G, Marchetti A, Dielectric constant enhancement in a silicone elastomer filled with lead magnesium niobate-leads titanate, Materials Science and Engineering C 27:110-1162, 2007
20. Gillen K T (1988), Effect of cross-links which occur during continuous chemical stress-relaxation, Macromolecules 21:442-446
21. Hossain M, Possart G, Steinmann P (2009a), A small-strain model to simulate the curing of thermosets, Computational Mechanics 43:769-779
22. Hossain M, Possart G, Steinmann P (2009b), A finite strain framework for the simulation of polymer curing. Part I: Elasticity, Computational Mechanics 44(5):621-630
23. Hossain M, Possart G, Steinmann P (2010), A finite strain framework for the simulation of polymer curing. Part II: Viscoelasticity and shrinkage, Computational Mechanics 46(3):363-375
24. Hossain M, Steinmann P (2014), Degree of cure-dependent modelling for polymer curing processes at small-strain. Part I: consistent reformulation, Computational Mechanics 53(4):777-787
25. Hossain M, Steinmann P (2015), Continuum Physics of Materials with Time-Dependent Properties: Reviewing the Case of Polymer Curing, Advances in Applied Mechanics, 48: 141-259
26. Hossain M, Saxena P, Steinmann P (2015), Modelling the mechanical aspects of the curing process of magneto-sensitive elastomeric materials, International Journal of Solids and Structures 58: 257-269
27. Hossain M, Saxena P, Steinmann P (2015), Modelling the curing process in magneto-sensitive materials: Rate-dependence and shrinkage, International Journal of Non-Linear Mechanics, 74:108-121
28. Hossain M, Chatzigeorgiou G, Meraghni F, Steinmann P, A multi-scale approach to model the curing process in magneto-sensitive polymeric materials, International Journal of Solids and Structures, 69-70:34-44, 2015
29. Hossain M, Vu D K, Steinmann P, Experimental study and numerical modelling of VHB 4910 polymer, Computational Materials Science, 59:65-74, 2012
30. Hossain M, Vu D K, Steinmann P, A comprehensive characterization of the electro-mechanically coupled properties of VHB 4910 polymer, Archive of Applied Mechanics, 85(4):523-537, 2014
31. Hossain M, Steinmann P (2018), Modelling electro-active polymers with a dispersion-type anisotropy, Smart Materials and Structures, 27(2):1-17
32. Heinrich C, Aldridge M, Wineman A S, Kieffer J, Waas A M, Shahwan K W (2013), The role of curing stresses in subsequent response, damage and failure of textile polymer composites, Journal of the Mechanics and Physics of Solids 61:1241-1264
33. Horgan C O, Saccomandi G (2004), Constitutive models for compressible nonlinearly elastic materials with limiting chain extensibility, Journal of Elasticity 77:123-138
34. Itskov M, On the accuracy of numerical integration over the unit sphere applied to full network models, Computational Mechanics, 57(5):859-865, 2016
35. Itskov M, Khiem V N, Waluyo S (2018), Electroelasticity of dielectric elastomers based on molecular chain statistics, Mathematics and Mechanics of Solids, DOI:10.1177/1081286518755846

36. Johlitz M, Steeb H, Diebels S, Chatzouridou A, Batal J and Possart W, Experimental and theoretical investigation of non-linear viscoelastic polyurethane systems, Journal of Materials Science, 42:9894-9904, 2007
37. Koh S J A, Keplinger C, Li T, Bauer S, Suo Z, Dielectric elastomer generators: How much energy can be converted?, Mechatronics, IEEE/ASME Transactions , 33-41, 16(1), 2011.
38. Kashani M R , Javadi S, Gharavi N, Dielectric properties of silicone rubber-titanium dioxide composites prepared by di-electrophoretic assembly of filler particles, Smart Materials and Structures, 19:1-7, 2010
39. Kussmaul B, Risse S, Kofod G, Wache R, Wegener M, McCarthy D N, Krueger H and Gerhard R, Enhancement of di-electric permittivity and electromechanical response in silicone elastomers: Molecular grafting of organic dipoles to the macromolecular network, Advanced Functional Materials 21:4589-4594, 2011
40. Keip M A, Steinmann P, Schröder J, Two-scale computational homogenization of electro-elasticity at finite strains, Computer Methods in Applied Mechanics and Engineering 278: 62-79, 2014
41. Kiasat M (2000), Curing shrinkage and residual stresses in viscoelastic thermosetting resins and composites, PhD Thesis, TU Delft, The Netherlands
42. Landgraf R, Scherzer R, Rudolph M, Ihlemann J, Modelling and simulation of adhesive curing processes in bonded piezo metal composites, Computational Mechanics 54(2):547-565, 2014
43. Landgraf R, Modeling and simulation of the curing of polymeric materials, PhD Dissertation, TU Chemnitz, Germany, 2015
44. Lion A, Höfer P (2007), On the phenomenological representation of curing phenomena in continuum mechanics, Archives of Mechanics 59:59-89
45. Liu B, Shaw M T, Electrorheology of filled silicone elastomers, Journal of Rheology 45:641-657,2011
46. Mehnert M, Hossain M, Steinmann P, On nonlinear thermo-electro-elasticity, Proceedings of the Royal Society/ A, 472 (2190), 20160170, 2016
47. Monk P, Finite Element Methods for Maxwell Equations, Oxford University Press, Clarendon (2003)
48. Molberg M, Crespy D, Rupper P, Nesch F, Manson J A E, Loewe C, Opris D M, High breakdown field dielectric elastomer actuators using encapsulated polyaniline as high dielectric constant filler, Adv Funct Mater, 20: 3280-3291, 2010
49. Miehe C, Göktepe S and Lulei F, A Micro-macro approach to rubber-like materials: Part-I, the non-affine micro-sphere model of rubber elasticity, Journal of the Mechanics and Physics of Solids, 52:2617-2660, 2004
50. Mahnken R, Thermodynamic consistent modeling of polymer curing coupled to viscoelasticity at large strains, International Journal of Solids and Structures 50(13): 2003-2021, 2013
51. Nateghi A, Dal H, Keip M A, Miehe C, An affine microsphere approach to modeling strain-induced crystallization in rubbery polymers, Continuum Mechanics and Thermodynamics, 30(3):485-507, 2018
52. Opris D M, Molberg M, Walder C, Ko Y S, Fischer B, Nuesch F A, New silicone composites for dielectric elastomer actuator applications in competition with acrylic foil Adv Funct Mater, 21 (2011), pp. 3531-3539
53. Oliva-Aviles A I, Aviles F, Sosa V, Electrical and piezoresistive properties of multi-walled carbon nanotube/polymer composite films aligned by an electric field, Carbon 49:2989-2997, 2011
54. Pandolfi A, Vasta M, Fiber distributed hyper elastic modelling of biological tissues, Mechanics of Materials,44:151-162, 2012
55. Brochu P, Pei Q, Advances in dielectric elastomers for actuators and artificial muscles, Macromolecular Rapid Communications 31:10-36, 2010
56. Reese S, Govindjee S (1998), A theory of finite viscoelasticity and numerical aspects, International Journal of Solids and Structures 35:3455-3482
57. Risse S, Kussmaul B, Krueger H, Kofod G, Synergistic improvement of actuation properties with compatibilized high permittivity filler, Adv Funct Mater, 22: 3958-3962, 2012

58. Risse S, Kussmaul B, Krueger H, Kofod G, A versatile method for enhancement of electromechanical sensitivity of silicone elastomers, RSC Adv, 2: 9029-9035, 2012
59. Romasanta L J, Lopez-Manchado M A, Verdejo R, Increasing the performance of dielectric elastomer actuators: A review from the materials perspective, Progress in Polymer Research, 51:188-211, 2014
60. Steinmann P, Hossain M, Possart G, Hyperelastic models for rubber-like materials: Consistent tangent operators and suitability of Treloar's data, Archive of Applied Mechanics, 82(9):1183-1217, 2012
61. Spencer A J M, Theory of invariants, in: Eringen, A. C. (ed.) Continuum Physics, Vol 1. Academic, New York, pp 239-353, 1971
62. Saxena P, Vu D K, Steinmann P, On rate-dependent dissipation effects in electro-elasticity, International Journal of Non-Linear Mechanics, 62:1-11, 2014
63. Saxena P, Pelteret J-P, Steinmann P, Modelling of iron-filled magneto-active polymers with a dispersed chain-like microstructure, European Journal of Mechanics-A/Solids 50: 132-151, 2015
64. Skacel P, Bursa J, Comparison of constitutive models of arterial layers with distributed collagen fibre orientations, Acta of Bioengineering and Biomechanics, 16(3):47-58, 2014
65. Tomer V, Randall C A, High field dielectric properties of anisotropic polymer-ceramic composites, J Appl Phys, 104: 074106/1-7, 2008
66. Thylander S, Microsphere-based modeling of electro-active polymers, PhD Dissertation, Lund University, Sweden, 2016
67. Vogel F, On the modeling and computation of electro- and magneto-active polymers, PhD Dissertation, Friedrich-Alexander-University Erlangen-Nuremberg, Germany, 2014.
68. Vu D K, Steinmann P, Numerical modeling of Non-linear electroelasticity, International Journal for Numerical Methods in Engineering, 70:685-704, 2007
69. Wissler M, Mazza E, Mechanical behavior of an acrylic elastomer used in dielectric elastomer actuators, Sensors and Actuators A, 134:494-504, 2007
70. Yang Ta-I, Kofinas P, Dielectric properties of polymer nanoparticle composites, Polymer, 48:791-798, 2009
71. Womersley R S, Interpolation and Cubature on the Sphere- UNSW Sydney web.maths.unsw.edu.au/ rsw/Sphere/ (Accessed on 11 June 2017)